PROCESSING DIGITAL X-RAY IMAGES AND ITS APPLICATION IN THE AUTOMATED VISUAL INSPECTION OF ALUMINUM CASTINGS

Domingo Mery
Departamento de Ingeniería Informática, Universidad de Santiago de Chile
Av. Ecuador 3659, Santiago de Chile
Email: dmery@ieee.org
http://www.diinf.usach.cl/~dmery

Abstract. *In this paper we present a brief overview of several techniques used in digital image processing for X-ray testing. The paper introduces the reader to the image processing theory employed in this NDT. Methodologies and principles will be outlined. Some application examples are given when inspecting aluminum castings followed by the limitations of the applicability of the methodologies used.*

Keywords. *X-Ray testing, automated inspection, aluminum castings.*

1. Introduction

Shrinkage as molten metal cools during the manufacture of die-castings, can cause non-homogeneous regions within the work piece. These are manifested, for example, by bubble-shaped voids or fractures. Voids occur when the liquid metal fails to flow into the die or flows in too slowly, whereas fractures are caused by mechanical stresses when neighboring regions develop different temperature gradients on cooling. Other possible casting defects include inclusions or slag formation.

Light-alloy castings produced for the automotive industry, such as wheel rims, steering knuckles and steering gear boxes are considered important components for overall roadworthiness. To ensure the safety of construction, it is necessary to check every part thoroughly (Mery et al, 2002).

Radioscopy rapidly became the accepted way for controlling the quality of die cast pieces through visual or computer-aided analysis of X-ray images. The purpose of this non-destructive testing method is to identify casting defects, which may be located within the piece and thus are undetectable to the naked eye. An example of such defects in a light-alloy wheel is shown in the X-ray image in Fig. 1.1. The automated visual inspection of castings is a quality control task to determine automatically whether a casting complies with a given set of product and product safety specifications.

Over the past decades radioscopic systems have been introduced in the automotive industry that detect flaws without human interaction, i.e. automatically (Boerner & Strecker, 1988; Filbert et al, 1987; Heinrich, 1988). Compared to a manual evaluation of X-ray images, automated detection of casting defects offers the advantages of objectivity and reproducibility for every test. Fundamental disadvantages of the methods proposed to date are the complexity of their configuration and inflexibility to any changes in the design of the work piece, which is something that people can accommodate easily. Research and development is, however, on going into automated adaptive processes to accommodate design modifications (Mery & Filbert, 2002a).

In recent years, automated radioscopic systems have not only raised quality, through repeated objective inspections and improved processes, but have also increased productivity and profitability by reducing labor costs (Brandt, 2000).

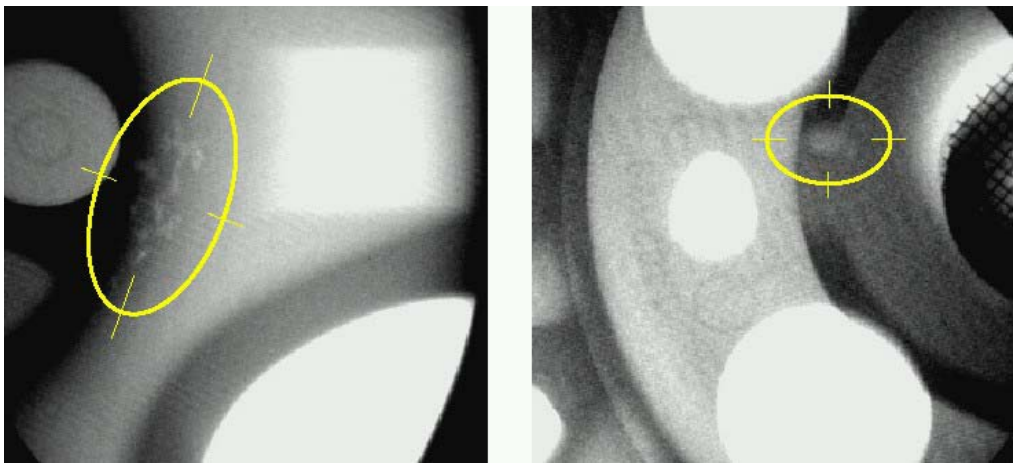

Figure 1.1: Voids in radioscopic images of aluminum wheels.

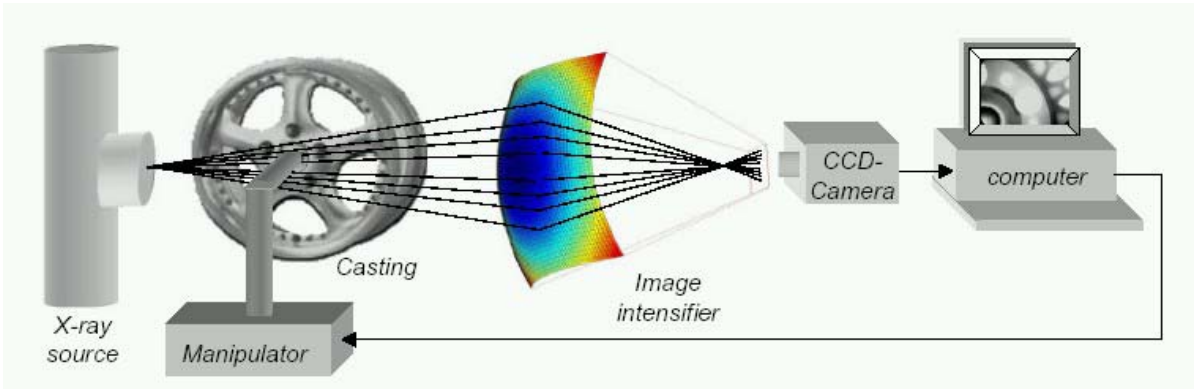

Figure 1.2: Schematic diagram of an automated X-ray testing stand.

The principle aspects of an automated X-ray inspection unit are shown in Fig. 1.2. Typically, it comprises the following five steps (Mery et al, 2001):

- a *manipulator* for handling the test piece,
- an *X-ray source*, which irradiates the test piece with a conical beam to generate an X-ray image of the test piece,
- an *image intensifier* which transforms the invisible X-ray image into a visible one,
- a *CCD camera* which records the visible X-ray image and
- a *computer* to process the digital image processing of the X-ray image and then classifies the test piece accepting or rejecting it. The computer may also control the manipulator for positioning the test piece in the desired inspection position, although this task is normally performed by a programmable logic controller (PLC).

At present, flat amorphous silicon detectors are used as image sensors in some industrial inspection systems (Jaeger et al, 1999; Bavendiek et al, 1998). In such detectors, using a semi-conductor, energy from the X-ray is converted directly into an electrical signal (without image intensifier). However, NDT using flat detectors is less feasible due to their higher cost in comparison to image intensifiers.

In this paper, we will discuss the use of image processing as a tool in the automated visual inspection of aluminum castings. The paper introduces the reader to the image processing theory employed when inspecting aluminum castings. Methodologies and principles will be outlined. Some application examples are given followed by the limitations of the applicability of the methodologies used. An early and extended version of this paper is presented in Section 2 of (Mery et al, 2003a).

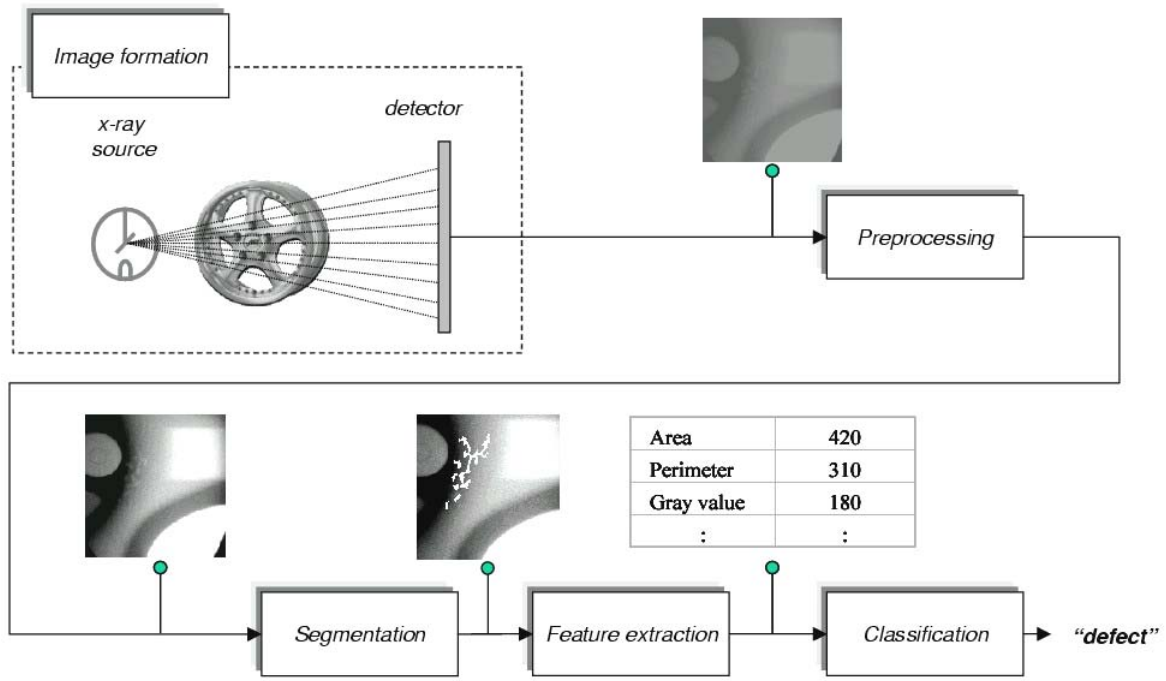

Figure 2.1: Phases of pattern recognition in automated flaw detection.

2. Digital Image Processing in X-ray Testing

Two classes of regions are possible in a digital X-ray image of an aluminum casting: regions belonging to regular structures of the specimen, and those relating to defects. In the computer-aided inspection of castings, our aim is to identify these two classes automatically using pattern recognition techniques.

The automatic pattern recognition process used in fault detection in aluminum castings, as shown in Fig. 2.1, consists of five steps:

- The first is *image formation*, in which an X-ray image of the casting under test is taken and stored in the computer.
- In the second step, *image preprocessing*, the quality of the X-ray image is improved in order to enhance the details of the X-ray image.
- The third one is called *image segmentation*, in which each region of the X-ray image is found and isolated from the rest of the scene.
- The fourth step is the *feature extraction*. This is where the regions are measured and some significant characteristics are quantified.
- The fifth step of the fault detection is *classification*. The extracted features of each region are analyzed and assigned to one of the classes ('regular structure' or 'defect').

In this Section we provide an overview of these five steps. Methodologies and principles will be outlined. Some application examples followed by limitations to the applicability of the used methodologies will be presented.

2.1 Image Formation

In X-ray examination, X-ray radiation is passed through the material under test, and a detector senses the radiation intensity attenuated by the material. A defect in the material modifies the expected radiation received by the sensor (Halmshaw, 1991). This phenomenon, called *differential absorption*, is illustrated in Fig. 2.2.

The contrast in the X-ray image between a flaw and a defect-free area of the specimen is distinctive. In an X-ray image we can see that the defects, such as voids, cracks or bubbles, show up as bright features. The reason is that the attenuation in these areas is shorter. Hence, according to the principle of differential absorption, the detection of flaws can be achieved automatically using image processing techniques that are able to identify unexpected regions in a digital X-ray image. A real example is shown in Fig. 2.3 which depicts two defects clearly.

The X-ray image is usually captured with a frame-grabber and stored in a matrix. An example of a digitized X-ray image is illustrated in Fig. 2.4. The size of the image matrix corresponds to the resolution of the image. In this example the size is 286 × 384 picture elements, or *pixels*. Each pixel has associated a *gray value*. This value is between 0 and 255 for a scale of $2^8 = 256$ gray levels. Here, '0' means 100% black and a value of '255' corresponds to 100% white, as illustrated in Fig. 2.5. Let matrix **x** be the digitized X-ray image, then the element $x(i,j)$ denotes the gray value of the i-th row of the j-th column, as shown in the matrix of Fig. 2.4. The eye is only capable of resolving around 40 gray levels (Castleman, 1996), however for the detection of defects in aluminum castings, gray level resolution must be a minimum of 256 levels. In some applications, $2^{16} = 65{,}536$ gray levels are used (Jaeger et al, 1999), which allows one to evaluate both very dark and very bright regions in the same image.

2.2 Preprocessing

The X-ray image taken must be preprocessed to improve the quality of the image before it is analyzed. In this Section, we will discuss preprocessing techniques that can remove noise, enhance contrast, correct the shading effect and restore blur deformation in X-ray images.

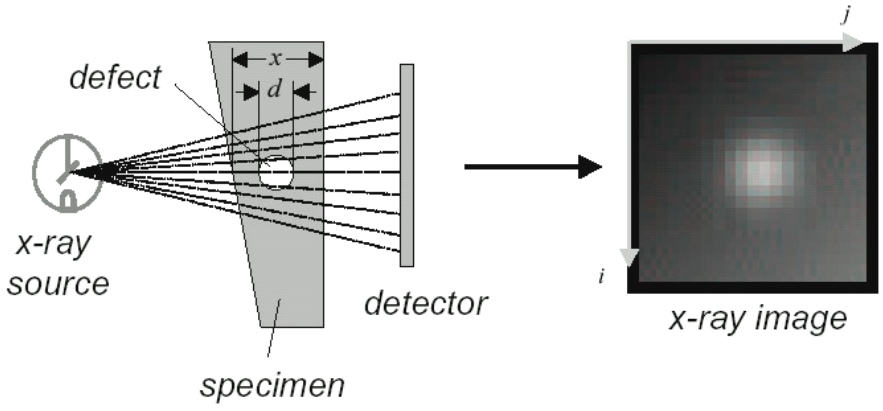

Figure 2.2: Differential absorption in a specimen.

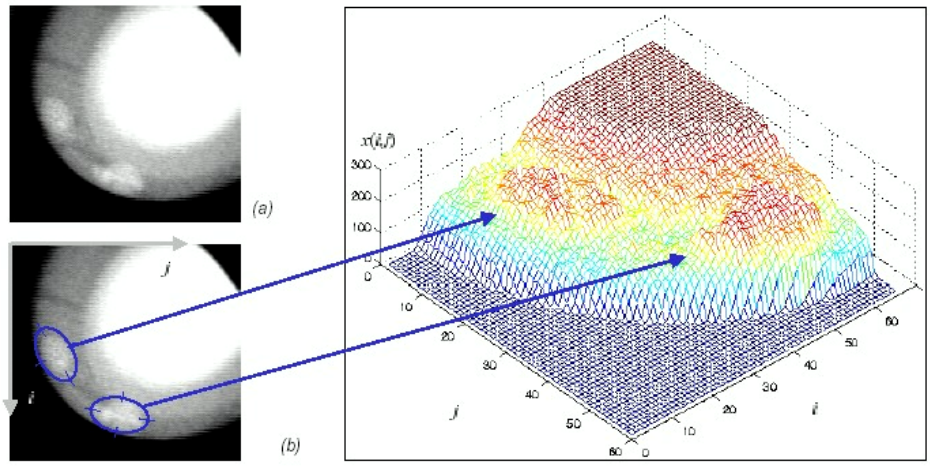

Figure 2.3: Image formation process: a) X-ray image of a wheel with two defects, b) 3D plot of the gray values of the image.

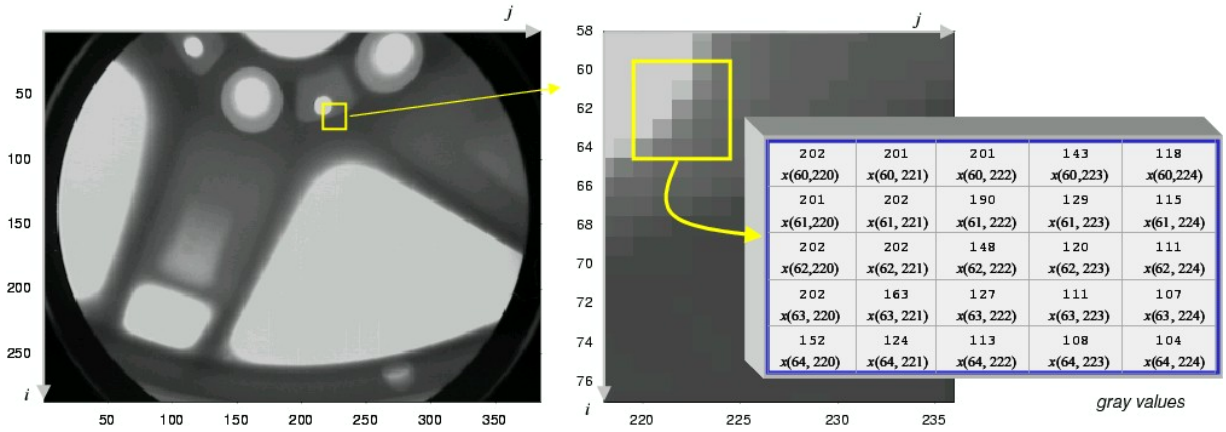

Figure 2.4: Digital X-ray image.

Figure 2.5: 256 gray level scale.

2.2.1 Noise Removal

Noise in an X-ray image can prove a significant source of image degradation and must be taken into account during image processing and analysis. In an X-ray imaging system, *photon noise* occurs given the quantum nature of X-rays. The number of photons striking any particular pixel in any time will be random. At low levels, however, the noise follows a Poisson law. The standard deviation of this distribution is equal to the square root of the mean. This means that the photon noise amplitude is signal-dependent.

Integration (or averaging) is used to remove X-ray image noise. This technique requires n stationary X-ray images. In this technique, the X-ray image noise is modeled using two components: the stationary component (that is constant throughout the n images) and the noise component (that varies from one image to the next). If the noise component has zero mean, by averaging the n images the stationary component is unchanged, while the noise pattern decreases by increasing n. Integrating n stationary X-ray images improves the signal-to-noise ratio by a factor of $\sqrt{n}$ (Castleman, 1996; Boerner & Strecker, 1988).

The effect of image integration is illustrated in Fig. 2.6 that uses n stationary images of an aluminum casting and shows the improvement in the quality of the X-ray image. The larger the number of stationary images n, the better the improvement. Normally, between 10 and 16 stationary images are taken ($10 \leq n \leq 16$).

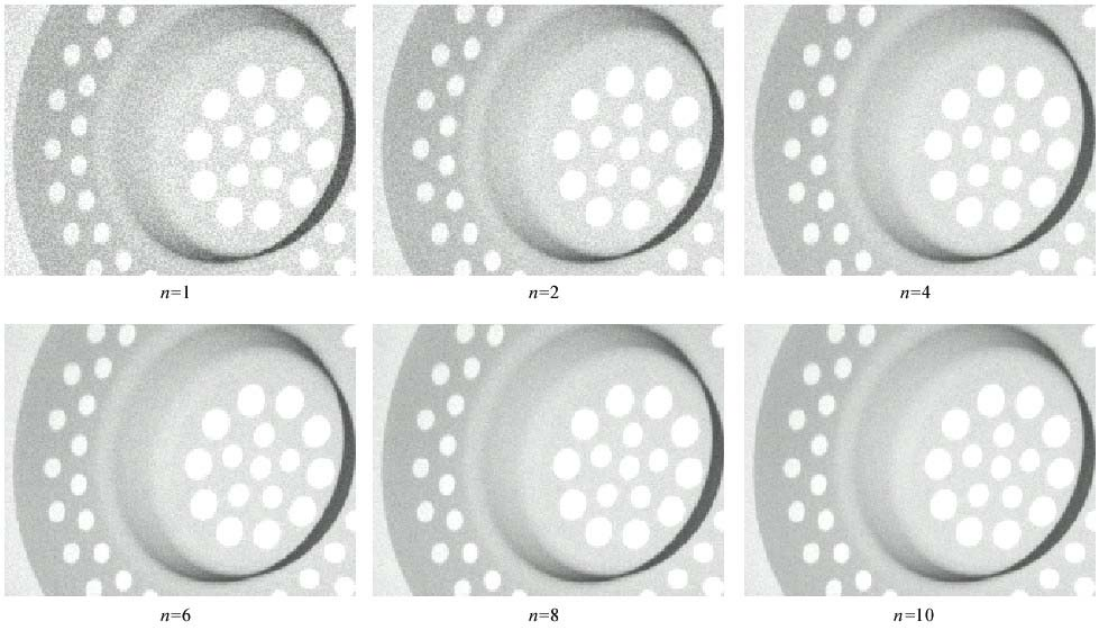

Figure 2.6: Noise removal after an averaging of *n* frames. The noise is reduced by factor $\sqrt{n}$.

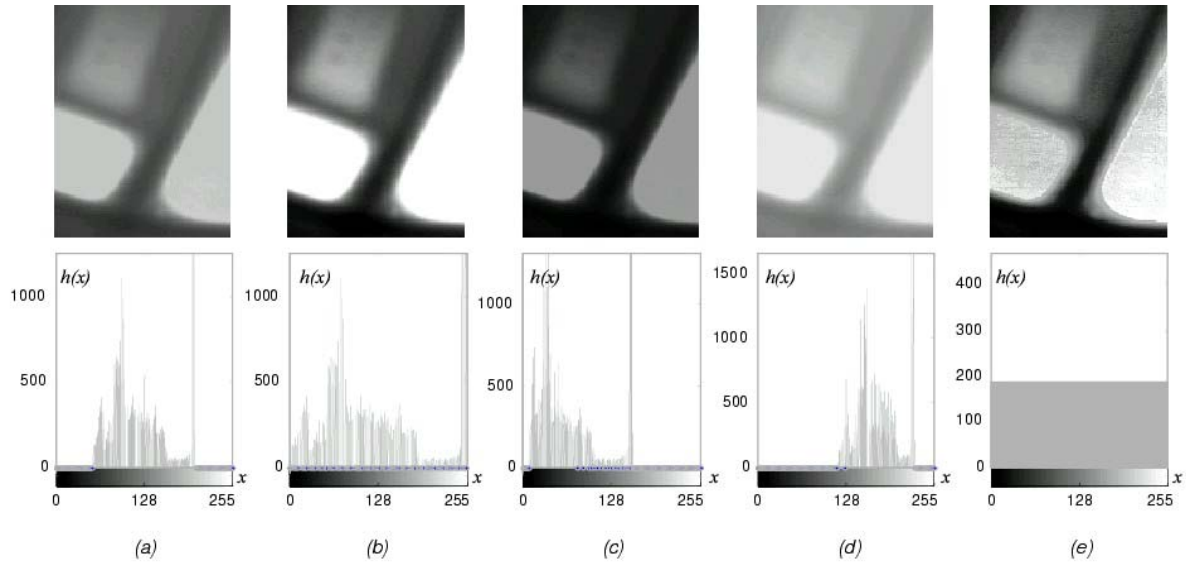

Figure 2.7: Contrast enhancement: a) original image, b) linear transformation ($\gamma = 1$), c) nonlinear transformation ($\gamma = 2$), d) nonlinear transformation ($\gamma = 1/2$), e) gray levels uniformly distributed.

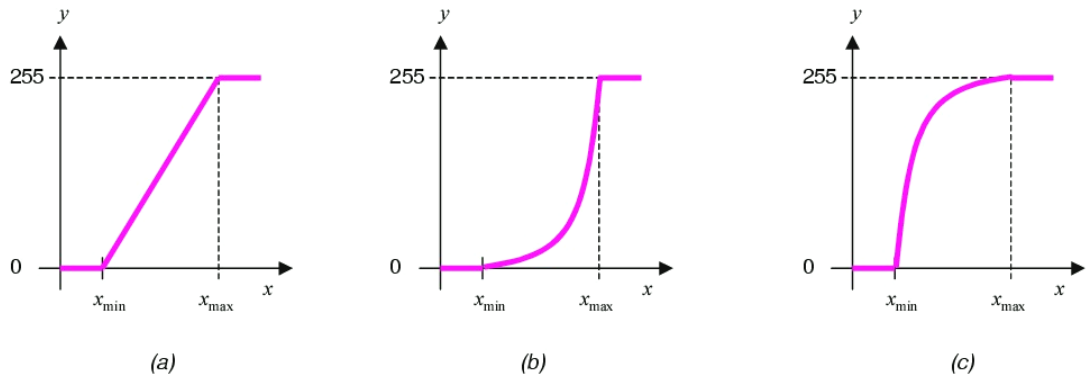

Figure 2.8: Plots showing different transformations of the gray levels: a) linear transformation (γ = 1), b) nonlinear transformation with $\gamma > 1$, c) nonlinear transformation with $\gamma < 1$. Input and output gray levels are *x* and *y* respectively.

2.2.2 Contrast Enhancement

The gray values in some X-ray images lie in a relatively narrow range of the gray scale. In this case, enhancing the contrast will amplify the differences in the gray levels of the image.

We use a gray level histogram to investigate an X-ray image's gray scale. The function summarizes the gray level information of an X-ray image. The histogram is a function $h(x)$ where x is a gray level and $h(x)$ denotes the number of pixels in the X-ray image that have a gray level equal to x. Fig. 2.7 shows how each histogram represents the distribution of gray levels in the X-ray images.

A transformation can be applied to modify the distribution of gray level in an X-ray image. Simple contrast enhancement can be achieved if we use a linear transformation which sets the minimal and maximal gray values of the X-ray image to the minimal and maximal gray value of the gray level scale respectively. Thus, the histogram is expanded to occupy the full range of the gray level scale. Figure 2.7b shows the result of the transformation applied to the X-ray image in Fig. 2.7a. We observe in the histogram of the enhanced X-ray image, how the gray levels expand from '0' to '255'. This linear transformation is illustrated in Fig. 2.8a, where the abscissa is the input gray value and the ordinate is the output gray value.

In a similar fashion, gray input image values can be mapped using a nonlinear transformation $y = f(x)$, as illustrated in Fig. 2.8b and 2.8c, whose results are shown in Fig. 2.7c and 2.7d, respectively. The nonlinear transformation is usually performed with a *γ-correction* (MathWorks, 1998). In these examples, if $\gamma > 1$ the mapping is weighted toward darker output values, and if $\gamma < 1$ the mapping is weighted toward brighter output values.

Finally, we present a contrast enhancement equalizing the histogram. Here, we can alter the gray level distribution in order to obtain a desired histogram. A typical equalization corresponds to the uniform histogram as shown in Fig. 2.7e. We see that the number of pixels in the X-ray image for each gray level is constant.

2.2.3 Shading Correction

A decrease in the angular intensity in the projection of the X-rays causes low spatial frequency variations in X-ray images (Boerner & Strecker, 1988; Heinrich, 1988). An example is illustrated in Fig. 2.9a, which shows an X-ray image of an aluminum plate with holes in it. Since the plate is of a constant thickness, we would expect to see a constant gray value for the aluminum part and another constant gray value for the holes. In fact, the X-ray image is darker at the corners. This deficiency can be overcome by using linear shading correction.

In this technique the gray value of each pixel of the input image $x(i,j)$ will be linear transformed according to $y(i,j) = a(i,j)\, x(i,j) + b(i,j)$ in order to remove the shading effect. The coefficients $a(i,j)$ and $b(i,j)$ are estimated by analyzing two real images $r_1(i,j)$ and $r_2(i,j)$ and the corresponding ideal images $i_1(i,j)$ and $i_2(i,j)$ as shown in Fig. 2.10. Thus, $i_k(i,j) = a(i,j)\, r_k(i,j) + b(i,j)$ for $k = 1,2$.

An example of this technique is illustrated in Fig. 2.9b. In this case we obtain only two gray values (with noise) one for the aluminum part and another for the holes of the plate.

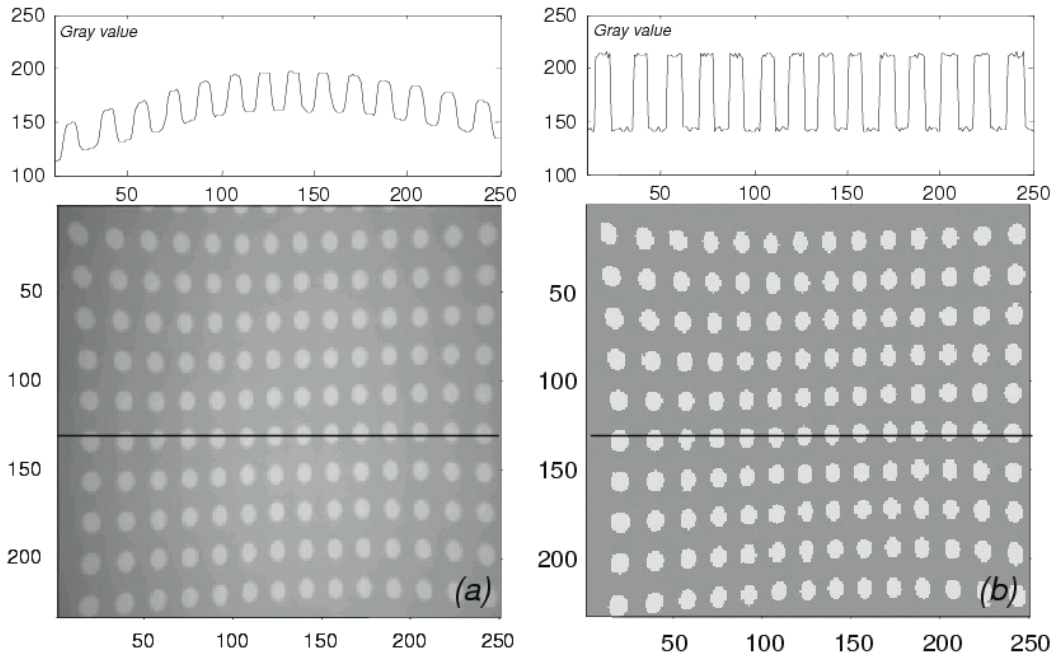

Figure 2.9: Shading correction: a) original image, b) image after shading correction. The corresponding gray values profiles of row number 130 are shown above the images.

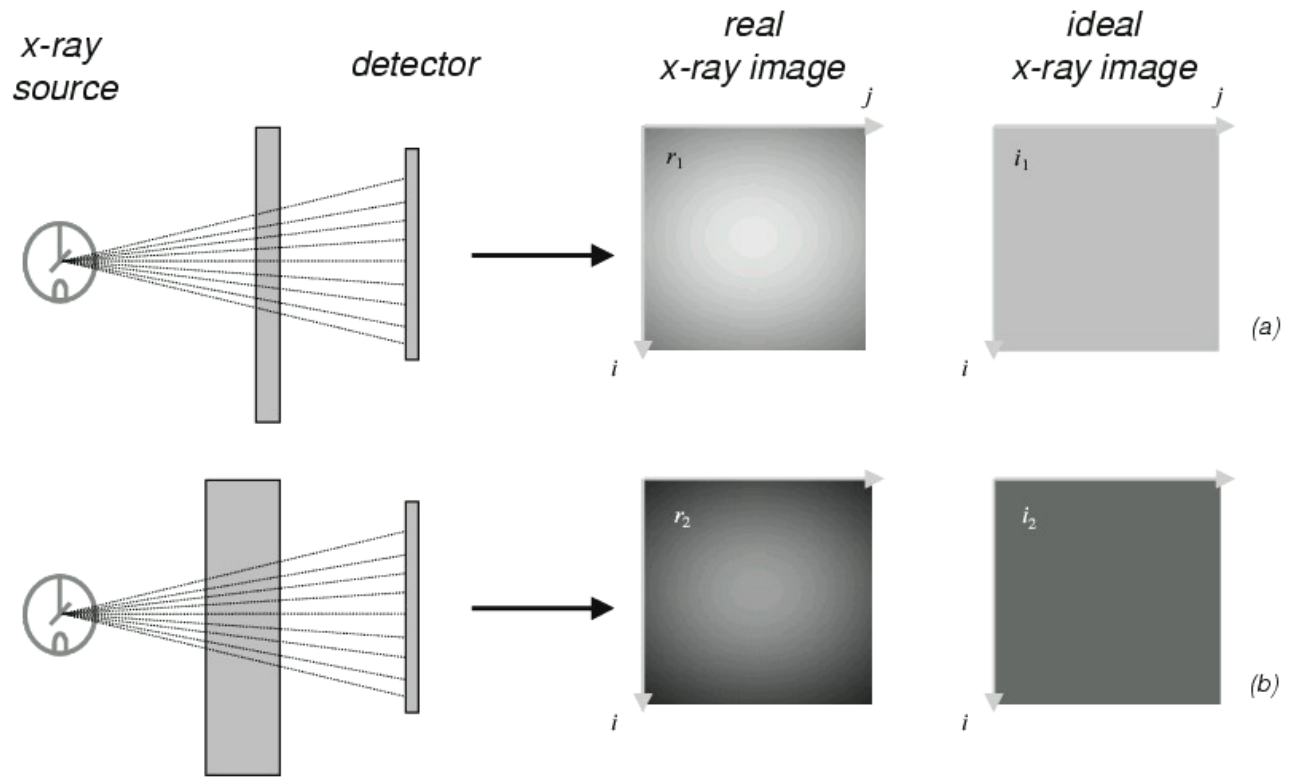

Figure 2.10: Shading correction: a) X-ray image for a thin plate, b) X-ray image for a thick plate.

2.2.4 Restoration of blur caused by motion

Image reconstruction involves recovering detail in severely blurred images, which is possible when the causes of the imperfections are known a-priori (Andrews & Hunt, 1977). This knowledge may exist as an analytical model, or as a-priori information in conjunction with knowledge (or assumptions) of the physical system that provided the imaging process in the first place (Bates & McDonnell, 1986). The purpose of restoration then is to estimate the best source image, given the blurred example and some a-priori knowledge.

An example is given in Fig. 2.11, where the blur caused by uniform linear motion is removed (Mery & Filbert, 2000b). In this case the method assumes that the linear motion corresponds to an integer number of pixels and is horizontally (or vertically) aligned with sampling raster. In these examples, the details of the aluminum castings are not discernable in the degraded images, but are recovered in the restored image. Other algorithms for restoration of X-ray images are given in (Purshke, 1989; Mery & Filbert, 2000a).

2.3 Segmentation

Image segmentation is defined as the process of subdividing an image into disjointed regions (Castleman, 1996). In image processing for detecting faults in castings, such regions correspond to potential defects and the background (or regular structures). While there are many methods for segmenting images, two approaches for segmenting potential defects in X-ray images are used widely within the nondestructive testing community. The first technique is based on median filtering while the second is a region-oriented method.

2.3.1 Median Filtering

2D Filtering is performed in digital image processing using a small neighborhood of a pixel $x(i,j)$ in an input image to produce a new gray value $y(i,j)$ in the output image, as shown in Fig. 2.12. A *filter mask* defines the input pixels to be processed by an *operator f*. The resulting value is the output pixel. The output for the entire image is obtained by shifting the mask over the input image.

Filtering out defects detected in an X-ray image of aluminum castings will provide a reference *defect-free* image. The defects are detected by finding deviations in the original image from the reference image. The problem is how one can generate a defect-free image from the original X-ray image. Assuming that the defects will be smaller than the regular structure of the test piece, one can use a low pass filter that does not consider the high frequency components of the image. However, if a linear filter is used for this task, the edges of the regular structure of the specimen are not necessarily preserved and many false alarms are raised at the edges of regular structures.

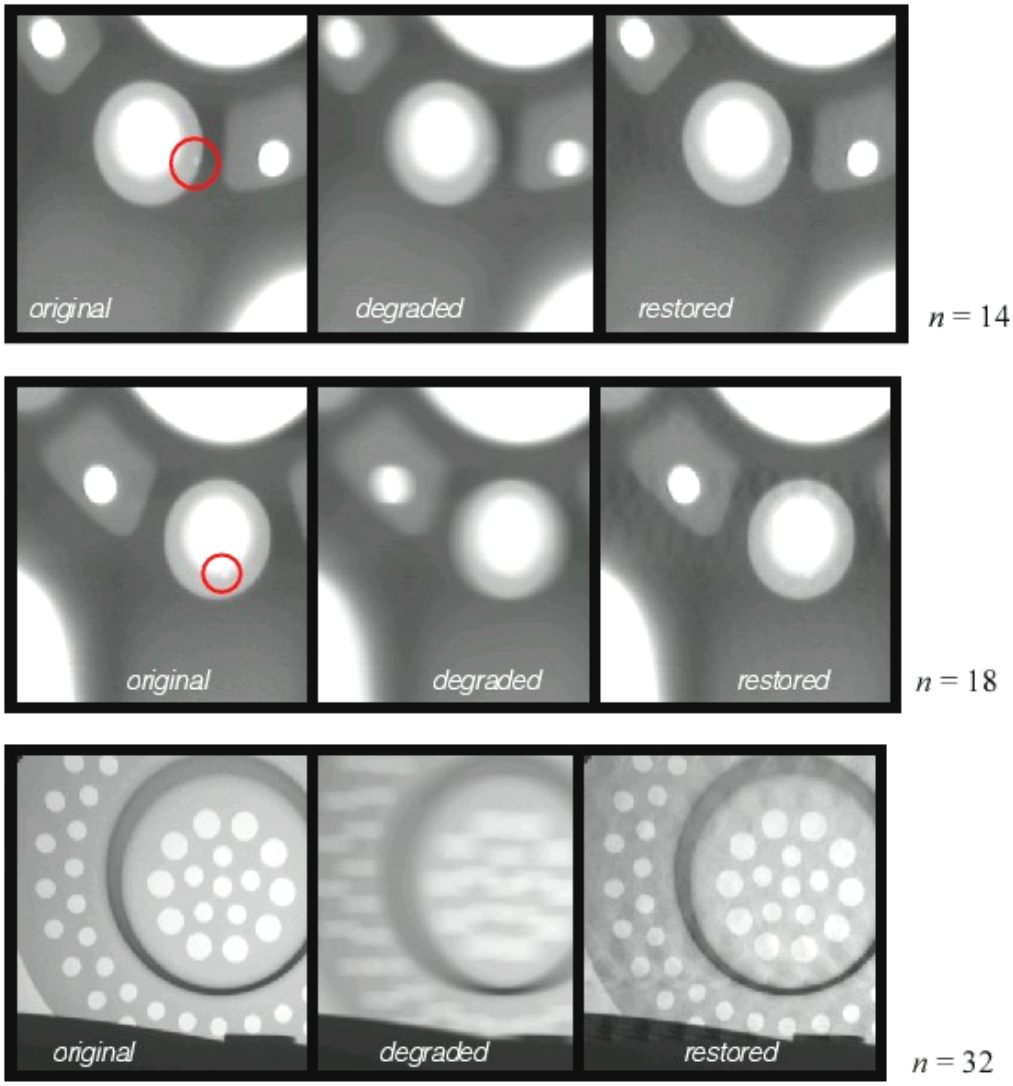

Figure 2.11: Restoration in simulated degraded X-ray images for different lengths of the blurring process in pixels.

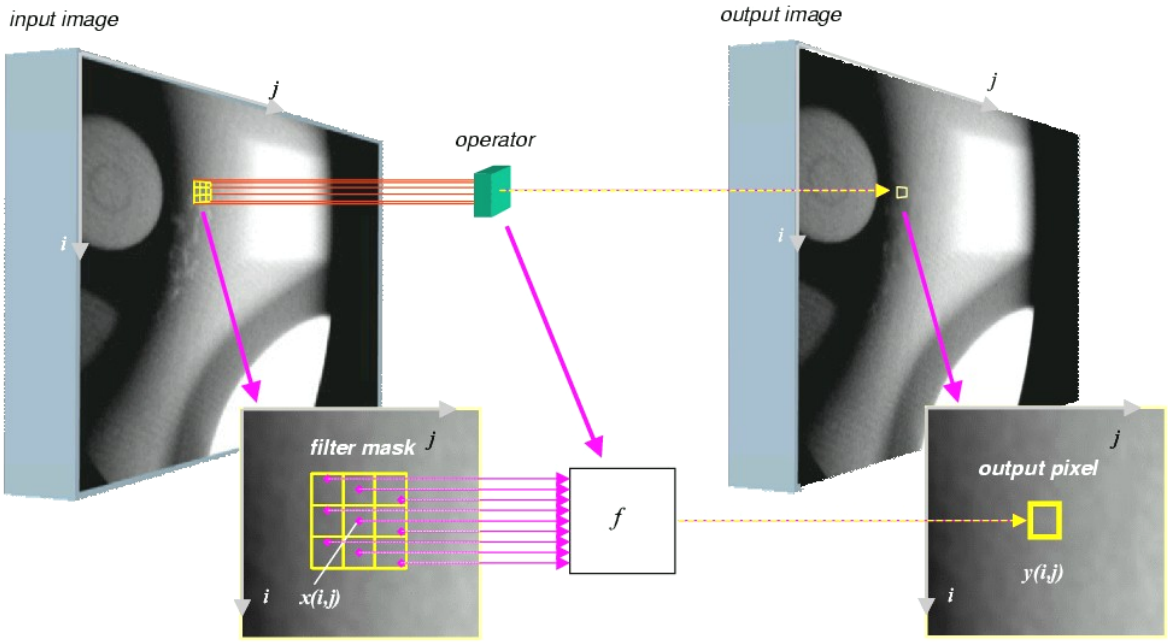

Figure 2.12: Digital image filtering.

Consequently, a nonlinear filter is used. Defect discrimination is normally performed with a *median filter*. The median filter is a ranking operator (and thus nonlinear) where the output value is the middle value of the input values ordered in a rising sequence (Castleman, 1996). For an even number of input numbers the median value is the arithmetic mean of the two middle values.

The application of a median filter is useful for generating the reference image because it smoothes noise yet preserves sharp edges, whereas other linear low pass filters blur such edges. Hence, it follows that small defects can be suppressed while the regular structures are preserved. Fig. 2.13 shows this phenomenon for a 1D example. The input signal *x* is filtered using a median filter with 9 input elements, and the resulting signal is *y*. We can see that structures of length *n* greater than four cannot be eliminated. The third column shows the detection *x*-*y*. Large structures of $n > 4$ not detected, as presented in the last two cases.

If the background captured by the median filter is constant, foreground structures could be suppressed if the number of values belonging to the structure is less than one half of the input value to the filter. This characteristic is utilized to suppress the defect structures and to preserve the design features of the test piece in the image.

An example for the application of a median filter on 2D signals (images) is shown in Fig. 2.14 and includes different structures and mask sizes compared to the effects of two linear low pass filters. One can appreciate that only the median filter manages to suppress the relatively small structures completely, whereas the large patterns retain their gray values and sharp edges.

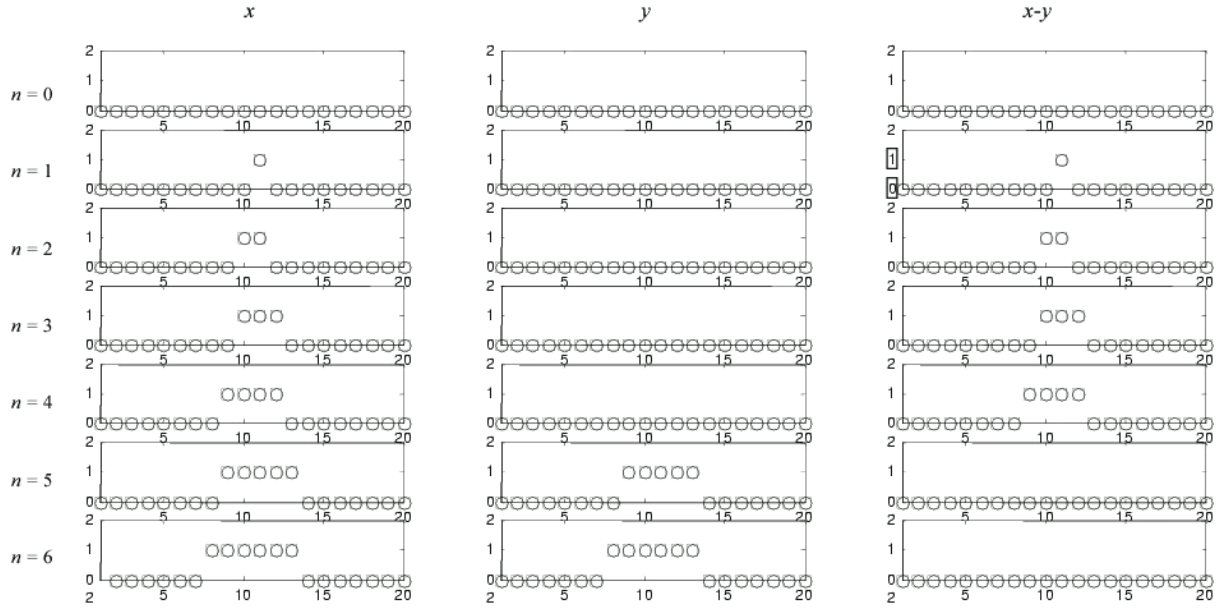

Figure 2.13: Median filter application on a 1D signal. The size of the median mask is nine.

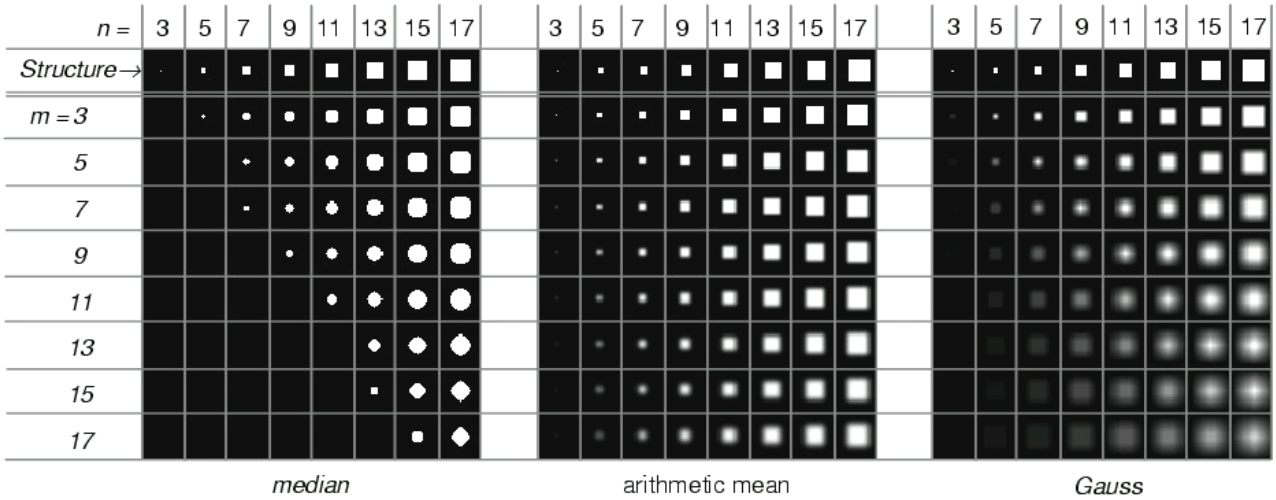

Figure 2.14: Median filter application on an $n \times n$ structure using an $m \times m$ quadratic mask compared to average and Gauss low pass filter application.

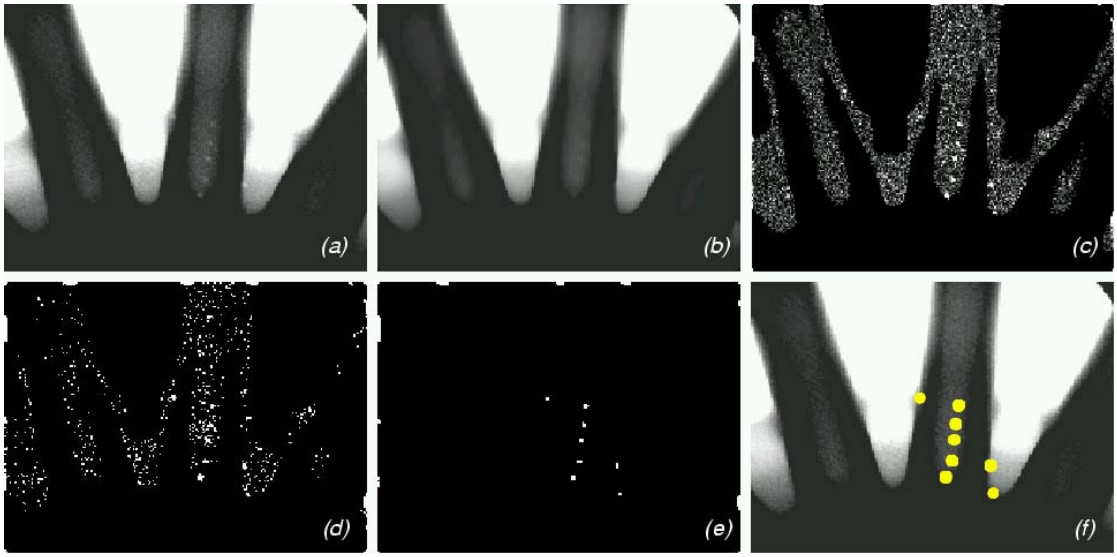

Figure 2.15: Defect detection using median filtering: a) original X-ray image, b) filtered X-ray image, c) difference image, d) binary image using a threshold, e) eroded image, f) dilated image superimposed onto original image.

The goal of the background image function, therefore, is to create a defect-free image from the test image. A real example is shown in Fig. 2.15. In this example, from an original X-ray image x we generate a filtered image y and a difference image $|x\text{-}y|$. By setting a threshold, we obtain a binary image whose pixels are '1' (or white), where the gray values in the difference image are greater than the selected threshold. After an erosion and dilation technique we discard isolated pixels that do not conform a large enough region (Castleman, 1996). The remaining pixels correspond to the detected flaws.

Locally variable masks are used during MODAN–filtering by adapting the form and size of the median filter masks to the design structure of the test piece (Heinrich, 1988; Filbert et al, 1987). This way, the design structure is maintained in the test image (and the defects are suppressed). Additionally, the number of elements in the operator are reduced in order to optimize the computing time by not assigning all positions in the mask (sparsely populated median filter (Castleman, 1996).

2.3.2 Edge Detection and Region Finding

This approach attempts to detect the potential defects in an X-ray image in two steps: *edge detection* and *region finding* (Mery & Filbert, 2002a). In the first step, the *edges* of the X-ray image are detected. The edges correspond to pixels of the image in which the gray level changes significantly over a short distance. The edges are normally detected using gradient operators. In the second step, the regions demarcated by the edges are extracted. The key idea of this two step based approach is that the existing defects present significant gray level changes compared to their surroundings. A Laplacian of Gaussian (LoG) kernel and a zero crossing algorithm (Castleman, 1996) can be used to detect the edges of the X-ray images. The LoG-operator involves a Gaussian low pass filter, which is good for the pre-smoothing of the noisy X-ray images. The LoG-kernel depends on parameter σ, which defines the width of the Gaussian function and, thus, the amount of smoothing and the edges detected (see Fig. 2.16). Using the LoG-kernel we calculate an image in which the edges of the original image are located by their zero crossing. The detected edges correspond to the maximal (or minimal) values of the gradient image. The binary edge image obtained should reproduce real flaws' closed and connected contours that demarcate *regions*. Fig. 2.17 illustrates the results obtained on an X-ray image by applying this method.

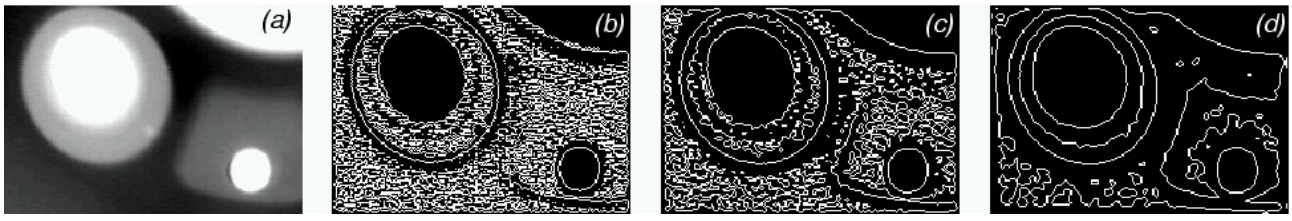

Figure 2.16: LoG-operator: a) original X-ray image; edge detection with b) $\sigma = 0$; 8 c) $\sigma = 1{,}3$ and d) $\sigma = 2{,}5$.

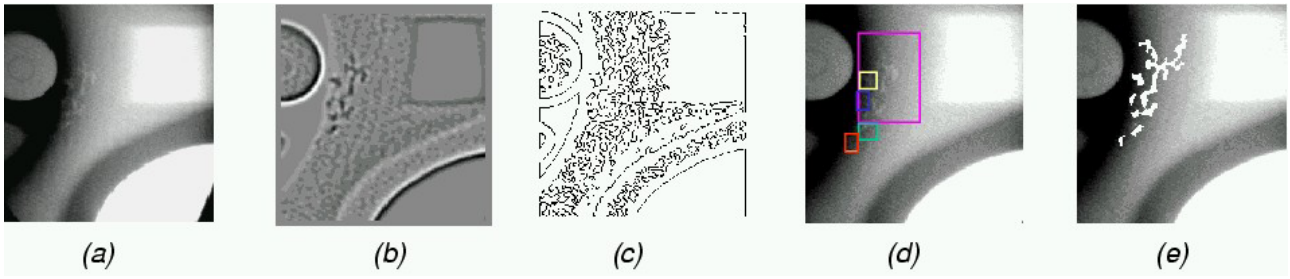

Figure 2.17: Segmentation by edge detection and region finding: a) original X-ray image, b) second derivate using LoG-operator, c) zero-crossing image, d) and e) detected regions.

2.4 Feature extraction and selection

Segmented potential defects frequently set off false alarms. An analysis of the segmented regions, however, can improve the effectiveness of fault detection significantly. Measuring certain characteristics of the segmented regions (*feature extraction*) can help us to distinguish the false alarms, although some of the features extracted are either irrelevant or are not correlated. Therefore, a *feature selection* must be performed. Depending on the values returned for the selected features, we can try to classify each segmented region in one of the following two classes: 'regular structure' or 'defect'. In this Section we concentrate on the extraction and selection of features, whereas in the next Section we will discuss the classification problem.

2.4.1 Feature extraction

In this section, we will mention features that are normally used in the classification of potential defects. A segmented region can be considered as a 2D and a 3D representation as shown in Fig. 2.18. For this reason, features are usually divided into two groups: *geometric* and *gray value* features. A detailed description of these features can be found in (Mery & Filbert 2002b; Mery et al, 2003b; Mery 2003).

The geometric features provide information about the size and the shape of the segmented potential flaw. The extracted geometric features can be: area, perimeter, height, width, roundness, Hu invariant moments, Flusser and Suk invariant moments, Fourier descriptors, and Gupta and Srinath moments, semi-minor and semi-major axis of ellipse fitted to the contour of the potential flaw, and Danielsson shape factor.

The gray value features provide information on the brightness of the segmented potential flaw. In this group, the extracted features are: mean gray value, mean gradient in the boundary, mean second derivate in the region, radiographic contrasts, contrasts based on *crossing line profiles*, invariant moments with gray value information, local variance, mean and range of the Haralick textural features (angular second moment, contrast, correlation, sum of squares, inverse difference moment, sum average, sum variance, sum entropy, entropy, difference variance, difference entropy, information measures of correlation and maximal correlation coefficient) based on the co-occurrence matrix in four different directions taken neighboring pixels separated by several distances, and components of the discrete Fourier transform, the Karhunen Loève transform and the discrete cosine transform taken from a window including potential flaw and neighborhood.

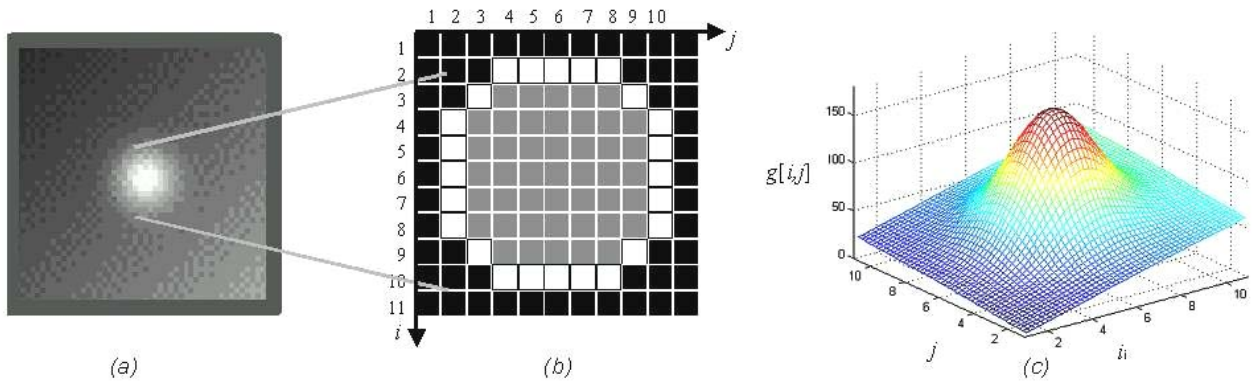

Figure 2.18: Example of a region: a) X-ray image, b) 2D representation of the segmented region, c) 3D representation of the gray values.

2.4.2 Feature selection

In feature selection we have to decide just which features of the regions are relevant to the classification. The *n* extracted features are arranged in an *n* -vector that can be viewed as a point in a n-dimensional space. In addition, each feature can be considered as a random variable with No samples. Each variable is normalized in order to obtain a zero mean and a standard deviation equal to one.

The key idea of the feature selection is to select a subset of *m* features ($m < n$) that leads to the smallest classification error. The selected *m* features are arranged in a new *m* -vector. The selection of the features can be done using *Sequential Forward Selection* (Jain et al, 2000). This method selects the best single feature and then adds one feature at a time that, in combination with the selected features, maximizes classification performance. The iteration is stopped once no considerable improvement in the performance is achieved on adding a new feature. By evaluating selection performance we ensure: *i)* a small intraclass variation and *ii)* a large interclass variation in the space of the selected features. For the first condition the intraclass-covariance matrix is used, and for the second the covariance matrix of each class.

The best features that separate the classes 'defects' and 'regular structures' are related to the contrast. (Mery, 2003; Mery et al, 2003b).

2.5 Classification

Once the proper features are selected, a classifier can be designed. Typically, the classifier assigns a feature vector $\mathbf{z}$ to one of the two classes: 'regular structure' or 'defect', that are assigned '0' and '1', respectively. In statistical pattern recognition, classification is performed using the concept of similarity: patterns that are *similar* are assigned to the same class (Jain et al, 2000, Fukunaga, 1990). Although this approach is very simple, a good metric defining the similarity must be established. Using a representative sample we can make a supervised classification finding a discriminant function $d(\mathbf{z})$ that provides us information on how similar a feature vector $\mathbf{z}$ is to the feature vector of a class. Fig. 2.19a shows the case for just one feature.

Some of the most important classifiers in statistical pattern recognition are: linear classifier, threshold classifier, nearest neighbor classifier, Mahalanobis classifier and Bayes classifier. The best classification was obtained with the Mahalanobis classifier (Mery & Filbert, 2002b).

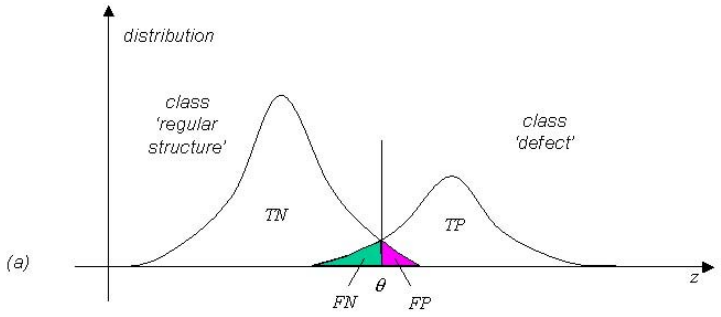

classified as →	regular structure	defect
Regular structures	TN	FP
Existining defect	FN	TP

(b)

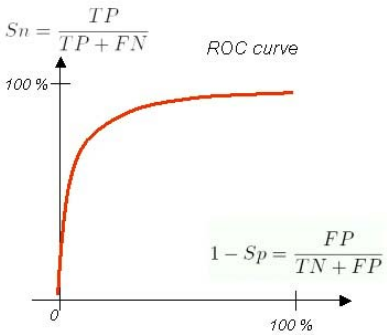

(c)

Figure 2.19: Classification: a) distribution of the classes using one feature *z*. The classification is performed by comparing *z* with a threshold θ ($z > \theta$ means class 'defect'. b) Table of classification performance. c) ROC Curve.

In order to obtain the feature that yields the best detection performance, the Receiver Operation Characteristic (ROC) curve is analyzed (Egan, 1975), which is a plot of the 'sensitivity' (S_n) against the '1-specificity' (1 - S_p) defined as:

$$S_n = \frac{TP}{TP + FN}, \qquad 1 - S_p = \frac{FP}{TN + FP} \tag{1}$$

where, as shown in Fig. 2.19b

- *TP* is the number of true positives (flaws correctly classified);
- *TN* the number of true negatives (regular structures correctly classified);
- *FP* is the number of false positives (false alarms, i.e., regular structures classified as defects); and
- *FN* is the number of false negatives (flaws classified as regular structures).

Ideally, $S_n = 1$ and $(1 - S_p) = 0$, i.e., all flaws are detected without flagging false alarms. The ROC curve permits to asses the detection performance at various operating points. The area under the ROC curve (A_z) is normally used as performance measure because it indicates how reliable the detection can be performed. A value of $A_z = 1$ gives perfect classification, whereas $A_z = 0{,}5$ corresponds to random guessing.

A classification can be tuned to a desired value of S_n. However, by increasing the S_n of the system, the 1- S_p would increase and vice versa as shown in Figure 2.19c. The ROC curve facilitates an assessment of recognition system performance at various operating points (Jain et al, 2000).

3. References

H. Andrews, B. Hunt, 1977. *Digital Restoration*. Englewood Cliffs, Pretince-Hall, NJ.

R. Bates M. McDonnell, 1986. *Restoration and Reconstruction*. The Oxford engineering science series, 16, Oxford University Press, NY.

K. Bavendiek, A. Krause, A. Beyer, 1998. Durchsatzerhöhung in der industriellen Röntgenprüfung – Eine Kombination aus innovativem Prüfablauf und optimierter Bildauswertung. In *DGZfP Jahrestagung*, volume Berichtsband 63.1, pages 301–306, Bamberg, 7-9 Sept. 1998.

H. Boerner H. Strecker, 1988. Automated X-ray inspection of aluminum casting. *IEEE Trans. Pattern Analysis and Machine Intelligence*, 10(1):79–91.

F. Brandt, 2000. The use of X-ray inspection techniques to improve quality and reduce costs. *The e-Journal of Nondestructive Testing & Ultrasonics*, 5(5).

K.R. Castleman, 1996. *Digital Image Processing*. Prentice-Hall, Englewood Cliffs, New Jersey.

J. Egan., 1975 *Signal detection theory and ROC analysis*. Academic Press, New York.

D. Filbert, R. Klatte, W. Heinrich, M. Purschke, 1987. Computer aided inspection of castings. In *IEEE-IAS Annual Meeting*, pages 1087–1095, Atlanta, USA.

K. Fukunaga, 1990, *Introduction to statistical pattern recognition*. Academic Press, Inc., San Diego, 2 edition.

R. Halmshaw, 1991. *Non-Destructive-Testing*. Edward Arnold, London, 2 edition.

W. Heinrich, 1988. *Automated Inspection of Castings using X-Ray Testing*. PhD thesis, Institute for Measurement and Automation, Faculty of Electrical Engineering, Technical University of Berlin. (in German).

Th. Jaeger, U. Heike, K. Bavendiek, 1999. Experiences with an amorphous silicon array detector in an ADR application. In *International Computerized Tomography for Industrial Applications and Image Processing in Radiology, DGZfP Proceedings BB 67-CD*, pages 111–114, Berlin, March 15-17 1999.

A.K. Jain, R.P.W. Duin, J. Mao, 2000. Statistical pattern recognition: A review. *IEEE Trans. Pattern Analysis and Machine Intelligence*, 22(1):4–37.

MathWorks Inc., 1998 *Image Processing Toolbox for Use with MATLAB: User's Guide*. The Math- Works Inc.

D. Mery, D. Filbert, 2000a. A fast non-iterative algorithm for the removal of blur caused by uniform linear motion in x-ray images. In *Proceedings of the 15th World Conference on Non- Destructive Testing (*15*th–WCNDT)*, Rome, Oct. 15-21 2000.

D. Mery, D. Filbert, 2000. Restauration bewegungsunscharfer Röntgenbilder. In *Berichtsband der Jahrestagung der Deutschen, Österreichischen und Schweizerischen Gesellschaft für Zerstörungsfreie Prüfung (DACH)*, Innsbruck, Austria, 29.-31. Mai 2000b.

D. Mery, Th. Jaeger, D. Filbert, 2001. Fully automated X-ray inspection: Non-destructive testing in industrial applications. *Materialprüfung*, 43(11-12):433–441. (in German).

D. Mery, D. Filbert, 2002a, Classification of Potential Defects in Automated Inspection of Aluminium Castings Using Statistical Pattern Recognition. In Proceedings of *8th European Conference on Non-Destructive Testing (ECNDT 2002)*, Jun. 17-21, Barcelona, Spain.

D. Mery, D. Filbert, 2002b, Automated Flaw Detection in Aluminum Castings Based on the Tracking of Potential Defects in a Radioscopic Image Sequence. *IEEE Transactions on Robotics and Automation*, 18(6): 890-901.

D. Mery, 2003, Crossing line profile: a new approach to detecting defects in aluminium castings, submitted to *Scandinavian Conference on Image Analysis (SCIA 2003)*, June 29 – July 2, Göteborg, Sweden.

D. Mery, D. Filbert, Jaeger, Th., 2003a, Image Processing for Fault Detection in Aluminum Castings. In *Analytical Characterization of Aluminum and Its Alloys*, Ed. C.S. MacKenzie and G.E. Totten, Marcel Dekker Inc. , New York (in Press).

D. Mery, R. da Silva, L.P. Calôba, J.M.A. Rebello, 2003b: Pattern Recognition in the Automatic Inspection of Aluminium Castings. Accepted in *International Symposium on Computerized Tomography for Industrial Applications and Image Processing in Radiology* (CTIP-2003), BAM, DGZfP, June 23-25, 2003, Berlin.

M. Purschke, 1989. *Verbesserung der Detailerkennbarkeit in Röntgendurchleuchtungsbildern durch digitale Bildrestauration*. PhD thesis, Institut für Allgemeine Elektrotechnik, Technische Universität Berlin.

8. Copyright Notice

Acknowledgment

This work was supported by the Departamento de Investigaciones Científicas y Tecnológicas of the Universidad de Santiago de Chile (grant DICYT 06-0119MQ).